J. Fluid Mech. (2010), *vol.* 658, *pp.* 63–88.
doi:10.1017/S0022112010001527

Foam mechanics: spontaneous rupture of thinning liquid films with Plateau borders

ANTHONY M. ANDERSON[1]†, LUCIEN N. BRUSH[2] AND STEPHEN H. DAVIS[1]

[1]Department of Engineering Sciences and Applied Mathematics, McCormick School of Engineering and Applied Science, Northwestern University, Evanston, IL 60208, USA

[2]Department of Materials Science and Engineering, University of Washington, Seattle, WA 98195, USA

(Received 13 July 2009; revised 21 March 2010; accepted 24 March 2010; first published online 10 June 2010)

Spontaneous film rupture from van der Waals instability is investigated in two dimensions. The focus is on pure liquids with clean interfaces. This case is applicable to metallic foams for which surfactants are not available. There are important implications in aqueous foams as well, but the main differences are noted. A thin liquid film between adjacent bubbles in a foam has finite length, curved boundaries (Plateau borders) and a drainage flow from capillary suction that causes it to thin. A full linear stability analysis of this thinning film shows that rupture occurs once the film has thinned to 'tens' of nanometres, whereas for a quiescent film with a constant and uniform thickness, rupture occurs when the thickness is 'hundreds' of nanometres. Plateau borders and flow are both found to contribute to the stabilization. The drainage flow leads to several distinct qualitative features as well. In particular, unstable disturbances are advected by the flow to the edges of the thin film. As a result, the edges of the film close to the Plateau borders appear more susceptible to rupture than the centre of the film.

Key words: breakup/coalescence, foams, instability

1. Introduction

In a foam, the gas phase is partitioned by a continuous liquid phase. We are interested in foams with a liquid fraction less than 10 %, such that the bubbles crowd each other. If a cross-section were taken of the foam, the bubbles would appear polygonal due to the close packing, with thin liquid bridges called 'lamellae' forming the edges of the polygons and 'Plateau borders' of nearly uniform curvature forming the corners. This is not an equilibrium configuration, as the foam will seek to lower its surface energy through coarsening. One mode of coarsening occurs from the diffusion of gas across lamellae, causing large bubbles to grow at the expense of smaller neighbouring bubbles. The other mode of coarsening occurs from the coalescence of adjacent bubbles, which results in abrupt changes in the total surface area of foam. The latter mode is dictated by two processes that are the focus of this paper: the thinning and breaking of the lamellae.

† Email address for correspondence: a-anderson@northwestern.edu

Since the Plateau borders are curved, surface tension causes a suction pressure which drains fluid from the lamellae, causing them to thin. The rate of thinning for a lamella composed of a pure liquid was obtained by Breward & Howell (2002) and Brush & Davis (2005), with the lamellar thickness decreasing as $h_L \sim t^{-2}$ for large times t. After sufficient thinning has occurred ($h_L \approx 10$–100 nm), long-range intermolecular forces due to van der Waals attractions become important and can lead to the spontaneous rupture of the film (Sheludko 1962, 1967). The change in thermodynamic properties (e.g. chemical potential) as a bulk phase becomes ultrathin in at least one of its dimensions is manifested in a 'disjoining pressure' ϕ (Derjaguin 1955). Using methods from quantum field theory, Lifshitz and his coworkers constructed a general macroscopic theory of van der Waals attractions for inhomogeneous medium calculable from the knowledge of its absorption spectra (Lifshitz 1956; Dzyaloshinskii & Pitaevskii 1959; Dzyaloshinskii, Lifshitz & Pitaevskii 1960). We are concerned with disjoining pressures $\phi \sim h_L^{-3}$, which arise from 'non-retarded' van der Waals attractions. The strongly divergent nature of these attractive forces as the film thickness tends to zero results in rapid acceleration towards rupture shortly after the onset of instability (Williams & Davis 1982; Erneux & Davis 1993); the evolution is locally self-similar near the rupture singularity (Ida & Miksis 1996; Vaynblat, Lister & Witelski 2001). Accurate predictions for the rate of coarsening in foam, as well as its lifetime, require proper characterization of the rupture conditions, where the film first becomes unstable to infinitesimal disturbances.

The lifetime of aqueous foams can be significantly prolonged with the addition of surfactant. On the one hand, a non-uniform distribution of surfactant along the interfaces results in Marangoni stresses which oppose drainage and slow thinning (this is described in detail by Breward & Howell 2002); if the gas–liquid interfaces become completely loaded with surfactant they are rendered immobile. On the other hand, electric double layers form along the interfaces of aqueous surfactant solutions, leading to repulsive forces which can counter the attractive van der Waals forces to prevent rupture (for non-ionic detergents, steric repulsion may be involved). The interplay between short-ranged repulsion and long-ranged attraction in ultrathin films is elaborated by Derjaguin–Landau–Verwey–Overbeek theory (Derjaguin & Landau 1941; Verwey & Overbeek 1948) and is responsible for the formation of metastable 'black films' (Overbeek 1960). We are interested in pure liquids with clean interfaces. Apart from their fundamental importance, this has applications to the coarsening of metallic foams, for which no surfactants are available. Metallic foams are inexpensive precursors to porous solids that are used in applications where weight considerations are important (for example, see Banhart 2001).

Vrij (1966) examined the spontaneous rupture of a free film with constant uniform thickness and infinite lateral extent using a static stability analysis. By expanding the fluctuations at the surfaces of the film in Fourier modes, Vrij's analysis formalized an earlier approach taken by Sheludko (1962). Such films are unstable to long waves that have wavelengths exceeding a critical value

$$\lambda_c = \left(\frac{4\pi^3\sigma}{A'}\right)^{1/2} h_0^2, \tag{1.1}$$

where h_0 is the film thickness, σ is the surface tension and A' is the Hamaker constant. According to this result, an unbounded film is always unstable. For a film of finite extent, a critical thickness for instability can be estimated from (1.1) by equating λ_c

to the length of the film. This basic result has been expanded to include the effects of surface active agents (Ivanov *et al.* 1970; Vrij *et al.* 1970; Ruckenstein & Jain 1974) as well as to liquid layers on a solid substrate (Ruckenstein & Jain 1974; Williams & Davis 1982).

While these results are instructive, they predict critical rupture thicknesses which are larger than what is measured experimentally (see Coons *et al.* 2003). There are several possible sources for this discrepancy. For example, films with finite length typically have curved boundaries and a drainage flow that causes thinning. This is certainly true for foam lamellae due to the presence of Plateau borders. In order to rigorously analyse the stability problem, one must confront a time-dependent and spatially non-uniform basic state. Gumerman & Homsy (1975) treated the linear stability of radially bounded thinning free films with tangentially immobile interfaces and a two-dimensional drainage flow computed from Reynolds' lubrication theory. A quasi-static (frozen-time) approximation was used to examine the instantaneous stability as the film thins. The critical thicknesses they obtained were smaller than those inferred from (1.1) and this stabilization was attributed to the drainage flow and finite film length. Sharma & Ruckenstein (1987) stressed that long-wavelength perturbations are particularly stabilized by the flow and argue that this leads to rupture modes with shorter wavelengths (about one-tenth of the film length). These results have spurred a number of related studies for draining films with tangentially immobile interfaces as reviewed by Coons *et al.* (2003). Here, we extend these results to the case of completely mobile interfaces.

A complete stability analysis for a film with finite length requires a prescription of the boundary conditions at the edges of the film. The analyses cited above have imposed these conditions artificially. However, given the long-wave nature of the van der Waals instability, one could expect the choice of boundary conditions to influence the predictions for rupture. To address this, we analyse the linear stability of a lamella coupled to its adjoining Plateau borders. Following the matched asymptotic analysis used by Brush & Davis (2005) (hereafter BD) to examine lamellar thinning of free films, we obtain two-dimensional composite solutions for the leading-order interfacial profile and fluid velocity and pressure fields. These approximate solutions are uniformly valid over a region of the fluid spanned by a lamella and its adjacent Plateau borders and serve as the basic state in the linear stability analysis. By systematically including the Plateau borders in this way, we present a physically correct method for imposing the conditions at the edges of the film. After formulating the problem in § 2.1, we review the matched asymptotic analysis of BD and construct the composite solutions in § 2.2.

The details of the linear stability analysis are given in § 3. We employ a frozen-time approximation to examine the instantaneous characteristics of the instability as the lamella thins. This approximation is commonly made when analysing the stability of time-dependent basic states, and its correct use requires that the evolution of the base state be slow relative to the growth and decay of the disturbances (Davis 1976). These conditions are not well met in the vicinity of marginal stability (Shen 1961), precisely where the critical thickness is obtained. To improve the frozen-time approximation we introduce an effective growth rate which depends on the rate of thinning. The growth rates and corresponding eigenfunctions are obtained through a numerical solution of the characteristic equations. Our approach uses an elliptic grid generation technique (Thompson, Warsi & Mastin 1985) which maps the physical domain into a rectangular computational domain, thus facilitating a discretization of the linear differential operator by finite differences.

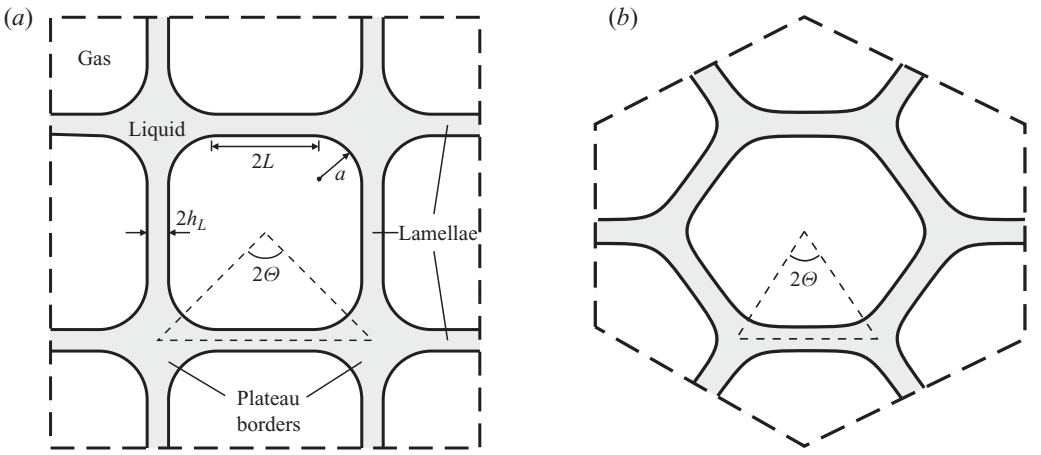

FIGURE 1. Two-dimensional periodic foam geometries with (*a*) square and (*b*) hexagonal symmetry. The hexagonal array satisfies Plateau's law, since three lamellae meet at the Plateau border.

Before presenting the results of these calculations, the stabilities of two idealized basic states are examined in § 4 to establish benchmarks for film rupture. Both benchmarks are for films of finite length and uniform thickness, but without Plateau borders. In the first benchmark, the film has a constant thickness, and in the second, the film is thinning in response to a drainage flow at a rate established by Plateau border suction. These two cases complement existing results for films with tangentially immobile interfaces mentioned above. The solutions from the full stability calculation are given in § 5, where we identify several new qualitative features of the instability and present the predictions for the critical thicknesses which are compared against the benchmarks. The results are chosen to illustrate the dependence of the critical lamellar thickness on Hamaker constant, surface tension, lamellar length and Plateau border radius of curvature. We conclude with a discussion in § 6.

2. Problem specification and basic state

We consider drainage and rupture occurring in two-dimensional lamellae. The same processes are also present in three-dimensional foams; however, the geometry is considerably more complex. Herein, we adopt the approach used by BD, who have analysed lamellar thinning by modelling the foam as a two-dimensional periodic array of bubbles, as shown in figure 1. The geometry is then characterized by four parameters: lamellar thickness $2h_L$, lamellar length $2L$, Plateau border radius of curvature a and angle Θ ($\Theta = \pi/4$ for a square array and $\Theta = \pi/6$ for a hexagonal array). Note that a hexagonal array has three lamellae joined at a Plateau border, in compliance with Plateau's law (Plateau 1873). The angle Θ does not play an important role in rupture, however, so we assume throughout that the foam has square symmetry.

The effects of gravity will be excluded because of the small volume fraction of liquid. This assumption was justified in the context of lamellar drainage (Breward & Howell 2002; Brush & Davis 2005) and earlier studies of film rupture have shown that gravity plays a non-essential role (Lucassen *et al.* 1970; Gumerman & Homsy 1975). With these specifications, it is sufficient to focus our efforts on a single lamella and its

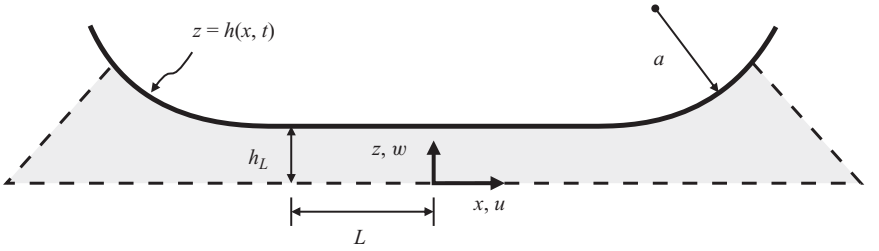

FIGURE 2. A lamella with adjoining Plateau borders. Shaded regions correspond to liquid and dashed lines are lines of symmetry which correspond to the dashed lines in figure 1.

adjoining Plateau borders, as shown in figure 2, where the dashed boundaries indicate lines of symmetry which coincide with the dashed boundaries of the triangular regions in figure 1. In the remainder of this section, we first formulate the free-boundary problem in the lamella and Plateau borders and then review previous work (Brush & Davis 2005) on lamellar thinning that defines a basic state for the subsequent linear stability analysis.

2.1. *Formulation*

We model the liquid phase as an incompressible Newtonian fluid with dynamic viscosity μ and density ρ, and the gas phase as a passive (quiescent) fluid of uniform pressure p_g. Non-dimensional variables are introduced by using the following scales: length L_0, time L_0/U_0, velocity U_0 and pressure $\mu U_0/L_0$, where $2L_0$ is the initial length of the lamella and U_0 is a velocity scale which characterizes lamellar drainage and will be defined later. Since the effects of inertia are not important in lamellar thinning (Brush & Davis 2005) nor at the onset of rupture (Ruckenstein & Jain 1974; Erneux & Davis 1993), we do not include them here. They must be included as the rupture processes develop beyond the linearized stability limit (Erneux & Davis 1993; Vaynblat *et al.* 2001). The equations for momentum and mass conservation are therefore given by the modified Stokes equations

$$\nabla(p+\phi) = \nabla^2 \boldsymbol{v}, \tag{2.1}$$

$$\nabla \cdot \boldsymbol{v} = 0, \tag{2.2}$$

where $\boldsymbol{v} = (u, w)$ is the fluid velocity with components u and w defined as in figure 2. In addition to the hydrodynamic pressure p, attractive van der Waals forces give rise to a disjoining pressure ϕ as the lamella approaches thicknesses at the submicrometre scale (10–100 nm). We consider only non-retarded van der Waals attractions modelled by

$$\phi(h) = \frac{A}{(2h)^3}, \tag{2.3}$$

which is a function of the total thickness of the liquid layer $2h$ and scaled by $A = A'/6\pi\mu U_0 L_0^2 > 0$, the non-dimensional Hamaker constant. The estimate $A' \approx 10^{-12}$ to 10^{-14} erg provides a typical energy scale for the (dimensional) Hamaker constant (Parsegian 2006).

The gas–liquid interface, located at $z = h(x, t)$, is modelled as a deformable boundary endowed with a constant surface tension σ. Here, the following kinematic condition is enforced:

$$w = h_t + uh_x, \tag{2.4}$$

along with normal and tangential stress balances

$$p - \boldsymbol{n} \cdot \left[\nabla \boldsymbol{v} + (\nabla \boldsymbol{v})^T\right] \cdot \boldsymbol{n} = C^{-1} \mathscr{K}(h), \tag{2.5}$$

$$\boldsymbol{t} \cdot \left[\nabla \boldsymbol{v} + (\nabla \boldsymbol{v})^T\right] \cdot \boldsymbol{n} = 0, \tag{2.6}$$

where $C = \mu U_0/\sigma$ is the capillary number, $\boldsymbol{n} = (-h_x, 1)/\sqrt{1+h_x^2}$ is the unit normal pointing into the gas phase, $\boldsymbol{t} = (1, h_x)/\sqrt{1+h_x^2}$ is the unit tangent and $\mathscr{K}(h) = -h_{xx}/(1+h_x^2)^{3/2}$ is twice the mean curvature. Note that, according to (2.5), p gives the non-dimensional pressure difference between the gas and liquid phases. To fully specify the problem, symmetry conditions are enforced at the remaining (dashed) boundaries. For instance, at the centreline $z = 0$, we require that $u_z = w = p_z = 0$.

2.2. *Basic state for lamellar thinning*

Using the problem formulation above, BD presented an analysis of lamellar thinning resulting from Plateau border suction and the findings are now reviewed to arrive at a basic state. The solution procedure follows a matched asymptotic analysis originally due to Bretherton (1961). In the limit of small capillary number ($C \ll 1$) there are three distinct scaling regions: the 'Plateau border regions' are capillary-static wherein the gas–liquid interface minimizes surface area, forming circular arcs of radius a; the 'lamellar region' is a viscous-dominated thin-film region which thins uniformly in response to a squeeze flow; and the 'transition regions' are narrow regions connecting the lamella and Plateau borders, in which both viscosity and capillarity are balanced. Leading-order solutions have been obtained in each region and we are interested in composite solutions for h, p, u and w which are uniformly valid over the entire region shown in figure 2.

Let h_0 and a_0 be the non-dimensional lamellar thickness and Plateau border radius, respectively, at time $t = 0$. Recall that all lengths are scaled by the lamellar length, so that $h_0 \ll 1$ measures the initial aspect ratio of the lamella. The asymptotic analysis outlined above yields an appropriate velocity scale for drainage $U_0 = (\sigma/\mu)\sqrt{h_0/a_0}$, which is consistent with our original assumption $C \ll 1$ provided that $h_0 \ll a_0$. With this velocity scale, the time scale for thinning is determined and the lamellar thickness h_L evolves according to the following ordinary differential equation:

$$\frac{\mathrm{d}h_L}{\mathrm{d}t} = -\frac{Q}{L}, \qquad Q = \frac{3}{8}\left(\frac{2a_0 h_L^3}{h_0 a}\right)^{1/2}, \qquad h_L(0) = h_0, \tag{2.7}$$

where Q is the drainage volume flow rate. The length L and radius a are determined for two distinguished geometric limits characterized by size of a_0 relative to h_0:

$$a_0 = O(1): \qquad L = 1, \quad a = a_0 \qquad \text{(semi-arid limit)}, \tag{2.8}$$

$$a_0 = O(\sqrt{h_0}): \quad L = 1, \quad a = \left[a_0^2 + \frac{2L(h_0 - h_L)}{\tan\Theta - \Theta}\right]^{1/2} \qquad \text{(arid limit)}. \tag{2.9}$$

BD show that drainage is initially slow in the arid limit since the Plateau borders must expand to accept fluid from the lamella. Ultimately, both limits exhibit the same long-time behaviour: $h_L/h_0 \sim t^{-2}$ and $a/a_0 \sim 1$. This is the regime where we perform the stability analysis.

A uniformly valid composite solution ψ^c is constructed in the standard way:

$$\psi^c = \psi_L + \psi_T + \psi_{PB} - \psi_{L\text{-}T} - \psi_{T\text{-}PB},$$

where ψ_L, ψ_T and ψ_{PB} are the solutions in the lamella, transition and Plateau border regions, respectively, and $\psi_{L\text{-}T}$ and $\psi_{T\text{-}PB}$ are the common parts which arise from

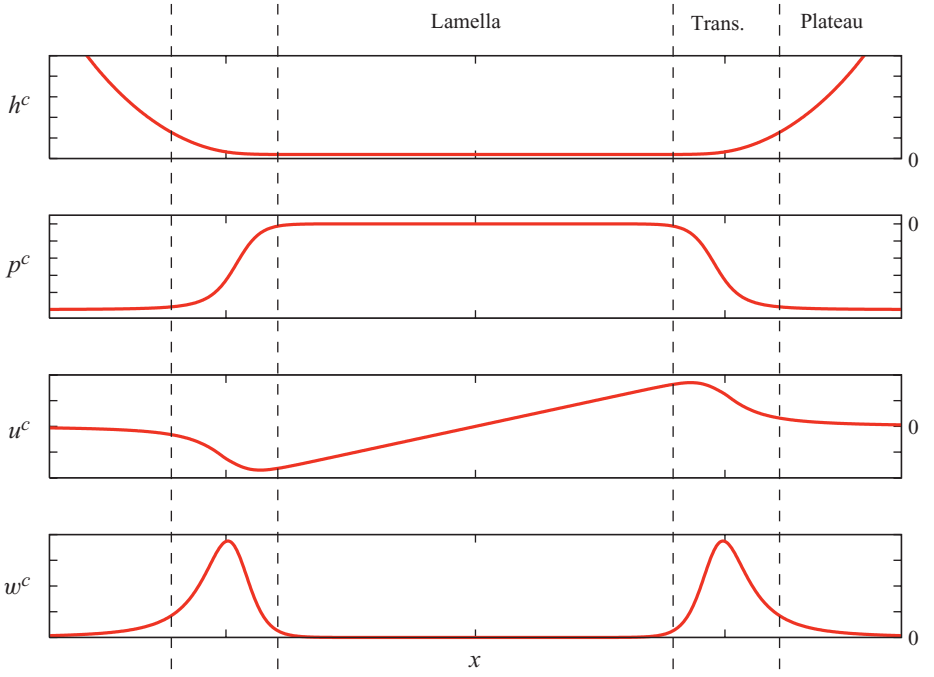

FIGURE 3. Composite solutions at a fixed time. These give an approximate basic state for the linear stability analysis.

matching ψ_L to ψ_T and ψ_T to ψ_{PB}, respectively. The interfacial profile is given by

$$h^c = \begin{cases} h_L\eta, & |x| \leqslant 1, \\ h_L\eta + \left[a - \sqrt{a^2 - (|x|-1)^2}\right] - \dfrac{(|x|-1)^2}{2a}, & |x| > 1, \end{cases} \tag{2.10}$$

and the field variables are given by

$$u^c = \frac{Q}{h_L}\begin{cases} -\eta^{-1}, & x < -1, \\ x + 1 - \eta^{-1}, & -1 \leqslant x < 0, \\ x - 1 + \eta^{-1}, & 0 \leqslant x \leqslant 1, \\ \eta^{-1}, & x > 1, \end{cases} \tag{2.11}$$

$$w^c = \frac{3}{4a}\sqrt{\frac{a_0}{h_0}}\left(\eta^{-3/2} - \eta^{-3}\right)z, \tag{2.12}$$

$$p^c = \frac{1}{2a}\sqrt{\frac{a_0}{h_0}}\left(\eta^{-3/2} + \eta^{-3} - 2\right), \tag{2.13}$$

where $h = h_L\eta$ is the film profile in the transition region, with η implicitly given by

$$2\sqrt{\eta} + \frac{1}{3}\ln\left(\frac{\eta - 2\sqrt{\eta} + 1}{\eta + \sqrt{\eta} + 1}\right) - \frac{2}{\sqrt{3}}\arctan\left(\frac{2\sqrt{\eta} + 1}{\sqrt{3}}\right) = \sqrt{\frac{2}{h_L a}}(|x| - 1). \tag{2.14}$$

The solutions (2.10)–(2.13) are plotted in figure 3 at a fixed time.

The composite film profile given by (2.10) leads to a flat lamella region and rounded Plateau borders, with a smooth monotonic transition in the intermediate region. The pressure is constant in both the lamella and Plateau borders, and the entire pressure drop between these regions is taken up in the transition region. This suction drives a uniform plug flow in the lamella, with the fluid moving into the Plateau borders where it comes to rest. Note that the transverse component of the fluid velocity only becomes appreciable in the transition region. This is required by continuity, since the film thickens as fluid enters the Plateau borders.

Finally, we point out that van der Waals attractions are a higher order effect in this basic state; Plateau border suction is the dominant effect which leads to thinning. If van der Waals attractions were strong enough to be included, lamellar drainage would be enhanced and thinning accelerated due to the additional conjoining pressure ϕ in the thin film. This assumption requires that $A = O(h_L^3)$ for all lamella thicknesses of interest. Whether or not this is true for physically relevant values of A therefore requires knowledge of the critical thickness at the onset of rupture. We return to this point in § 6 after we have presented the results of the linear stability analysis.

3. Linear stability analysis

In this section, we give the details for the linear stability analysis of the approximate basic state $\bar{\psi} \approx \psi^c \equiv \{h^c, u^c, w^c, p^c\}$ given by (2.10)–(2.13). This base state is a time-dependent flowing and spatially non-uniform state characterized concisely at any instant in time by the geometric quantities h_L and a which evolve according to (2.7) and (2.8) in the semi-arid limit and (2.7) and (2.9) in the arid limit. For the purposes of studying film rupture, only the long-time (self-similar) behaviour of these quantities is of interest, where film thicknesses approach the submicrometre scale and the Plateau border radius of curvature approaches a constant value. The distinction between semi-arid and arid foams is not necessary in the linear stability analysis, though it is important that a distinction be made when discussing the time to rupture.

Consider now the infinitesimal perturbations to the basic state $\hat{\psi} = \psi - \bar{\psi}$. Such disturbances occur naturally due to the presence of spontaneous thermal fluctuations at the surfaces of the thin liquid films (Vrij & Overbeek 1968). The linearization of the governing equations and boundary conditions (2.1)–(2.6) with respect to these perturbations leads to a linear stability problem of the form

$$B\hat{\psi}_t = \mathscr{L}(x, z, t; \text{parameters})\hat{\psi}, \tag{3.1}$$

where $\mathscr{L}$ is a linear differential operator and the operator B is simply used to indicate that the left-hand side is present for the linearized kinematic condition, but is otherwise zero. Formally, (3.1) is derived by linearizing about an exact solution $\bar{\psi}$ and using the composite solutions ψ^c to approximate the coefficients of the operator $\mathscr{L}$. The explicit form of the linear stability equations are given in the Appendix along with the details of the linearization. These equations are written in general curvilinear coordinates to facilitate a numerical solution which is described in further detail below.

In principle, film rupture could be analysed by prescribing initial conditions with (3.1) and integrating the full initial-value problem. An alternative and more instructive approach is to examine the characteristics of the instability. This is facilitated by a 'frozen-time' approximation, whereby the basic state is assumed to evolve slowly

relative to the growth of the perturbations, thus permitting solutions of the form

$$\hat{\psi} = \Psi(x, z, t^*)\mathrm{e}^{\sigma(t^*)t}, \tag{3.2}$$

where the basic state is evaluated at the time t^*, but t^* is regarded as a parameter (Davis 1976). Introducing this ansatz into (3.1) leads to the differential eigenvalue problem

$$\sigma(t^*)B\Psi = \mathscr{L}(x, z, t^*; \text{parameters})\Psi, \tag{3.3}$$

for the instantaneous growth rate $\sigma(t^*)$ and eigenfunctions $\Psi(x, z, t^*)$. The independent parameters of (3.3) are $h_L(t^*)$, a and A. To quantify the strength of van der Waals attractions we use the Sheludko number,

$$S \equiv AC = \frac{A'}{6\pi\sigma L_0^2}, \tag{3.4}$$

in place of A because of its central importance in studies of film rupture (Sheludko 1962).

The frozen-time approximation has been frequently used in earlier analyses of rupture for thinning films (Vrij 1966; Vrij & Overbeek 1968; Ivanov *et al.* 1970; Ruckenstein & Jain 1974; Gumerman & Homsy 1975); however, the underlying assumptions must break down in the vicinity of marginal stability where the principle modes for rupture are slowly growing or decaying (Shen 1961). The time dependence of the basic state must be accounted for when predicting the onset of rupture. For this purpose, we define an 'effective growth rate' for perturbations

$$\sigma_E(t^*) \equiv \frac{\mathrm{d}}{\mathrm{d}t}\left[\ln(\hat{h}) + \ln(h_L)\right]_{t=t^*} = \sigma(t^*) - \frac{Q(t^*)}{h_L(t^*)}, \tag{3.5}$$

which modifies the growth rate for perturbations computed with the frozen-time approximation by the rate of lamellar thinning, with the drainage rate Q given by (2.7). The growth of perturbations is effectively delayed as the film continues to thin in the vicinity of marginal stability. This definition follows from a related study by Burelbach, Bankoff & Davis (1988) who examined the van der Waals instability of films thinning due to evaporation. There, the fully time-dependent linear stability problem was analysed, and the effective growth rate (3.5) was found to properly characterize the marginal stability.

The spatially non-uniform basic state renders a linear operator $\mathscr{L}$ with variable coefficients and so we pursue a numerical solution of (3.3). Our strategy is to map the linearized physical domain into a rectangular computational domain to facilitate a discretization of the linear operator using finite-difference methods and the conversion of (3.3) into a matrix eigenvalue problem. For this reason, we express the linear stability equations in a boundary-fitted curvilinear coordinate system in the Appendix. The coordinate mapping is obtained numerically using an elliptic grid generation technique capable of producing a high-quality nearly orthogonal computational grid (Thompson *et al.* 1985). A sample grid is shown in figure 4.

Centred differences are used at the interior grid points and one-sided differences are used at the boundaries to discretize (A 1)–(A 8) as well as to compute the metric quantities that appear as coefficients in these equations. Discretization produces a generalized eigenvalue problem $\boldsymbol{A\Psi} = \sigma\boldsymbol{B\Psi}$, where $\boldsymbol{A}$ is the matrix which approximates the operator $\mathscr{L}$, $\boldsymbol{B}$ is a matrix corresponding to the operator B and $\boldsymbol{\Psi}$ is the vector of unknowns defined at grid points. For an $M \times N$ grid (see figure 4), there are $3MN + M$ unknowns. When using an approximately uniform distribution

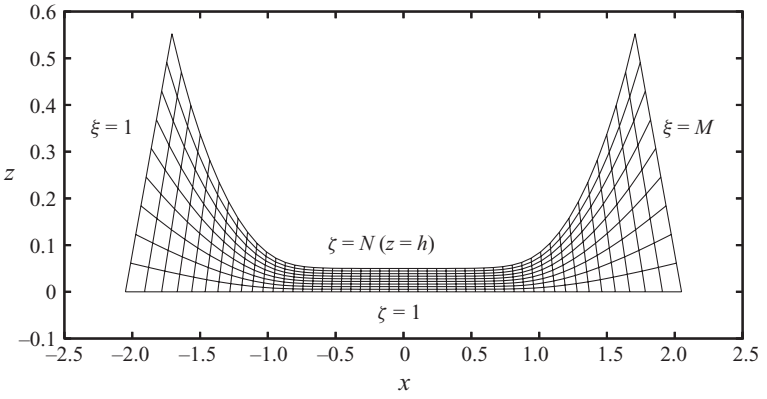

FIGURE 4. Boundary-fitted curvilinear coordinates (ξ, ζ) created using an elliptic grid generator with $M = 50$ and $N = 10$.

of grid points along the film, a grid with $M = 200$ and $N = 50$ is found to give sufficient numerical resolution. Floating-point precision plays a very crucial role in the calculations due to the disparate scales in the basic state. In order to control round-off error, we find it necessary to use 128-bit (quadruple) precision floating-point arithmetic. Interestingly, in a closely related problem involving the dewetting of a fluid film of finite extent, Diez & Kondic (2007) also report that quadruple precision was required to avoid spurious effects from round-off error.

We use an implicitly restarted Arnoldi method with spectral shift to solve the generalized eigenvalue problem. A software implementation of this method is provided by ARPACK (see Lehoucq, Sorensen & Yang 1998), which is available at the Netlib Repository (`www.netlib.org`). This method is capable of computing the extremal eigenvalues and eigenfunctions of large sparse unsymmetric matrices, which makes it well suited for the present stability calculations. We use the sequential version of the Multifrontal Massively Parallel Sparse direct Solver (MUMPS) software library (Amestoy *et al.* 2000) for sparse storage and matrix factorizations. With these sparse methods, it is feasible to accurately compute the neutral stability conditions across a wide range of parameter values, as demonstrated later in § 5.

4. Benchmarks for film rupture

Before presenting the results of the linear stability calculations discussed in the previous section, it is instructive to establish benchmarks for film stability by considering idealized basic states. Consider the film shown in figure 5, which is a uniform film of finite length that is thinning due to a drainage flow. Using the non-dimensionalization from § 2.1, solutions for the film thickness $\bar{h}$ and the x-component of velocity $\bar{u}$ are given by

$$\frac{\mathrm{d}\bar{h}}{\mathrm{d}t} = -Q(t), \quad \bar{u}(x,t) = \frac{Q(t)x}{\bar{h}(t)}, \tag{4.1}$$

where $\bar{h}(0) = h_0$ and $Q(t)$ is the flow rate of the fluid out of each end of the film. These solutions capture some key features of the full basic state derived in § 2.2 without considering Plateau borders. The two cases $Q = 0$ and $Q > 0$ provide important benchmarks for film rupture. The former case was treated in earlier analyses that considered a spatially extended film of constant thickness (Vrij 1966; Ruckenstein

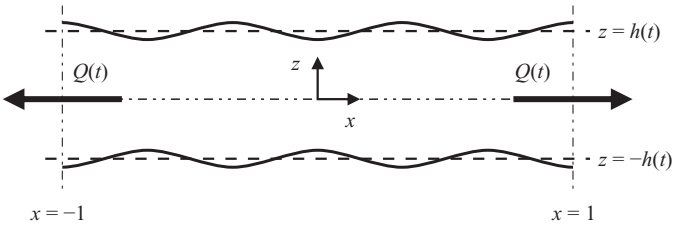

FIGURE 5. A uniform squeeze film which is draining at a rate Q.

& Jain 1974). These will be adapted here for a film with finite length. In the latter case with flow, a similar analysis was performed by Gumerman & Homsy (1975) for a thinning film with tangentially immobile interfaces; here, we present results for completely mobile interfaces.

Since the films under consideration are thin ($\bar{h} \ll 1$) and we are interested in long-wave instabilities, the linear stability analysis is performed using an asymptotically simplified form of the governing equations and boundary conditions (2.1)–(2.6) (Erneux & Davis 1993). We introduce the following rescaled variables

$$X = x, \quad Z = z/h_0, \quad T = t, \quad H = h/h_0, \quad U = u, \quad W = w/h_0, \quad \bar{Q} = Q/h_0,$$

and parameters

$$\bar{A} = A/h_0^3, \quad \bar{C} = C/h_0,$$

where all rescaled quantities are assumed to be $O(1)$ as the initial aspect ratio $h_0 \to 0$. This leads to the following long-wave equations for $H = H(X, T)$ and $U = U(X, T)$:

$$H_T + (UH)_X = 0, \tag{4.2}$$

$$4(HU_X)_X + \bar{C}^{-1} H H_{XXX} - \bar{A} H \Phi_X = 0, \tag{4.3}$$

where $\Phi = 1/(2H)^3$ is the rescaled van der Waals potential.

The basic state given by (4.1) is similarly rescaled: $\bar{H} = \bar{h}/h_0$ and $\bar{U} = \bar{u}$. It is readily shown that $\bar{H}$ and $\bar{U}$ are exact solutions to (4.2) and (4.3) with an appropriate choice of boundary conditions at the edges of the film. The linear stability analysis proceeds by introducing infinitesimal perturbations $\hat{H} = H - \bar{H}$ and $\hat{U} = U - \bar{U}$ and linearizing (4.2) and (4.3) to give

$$\hat{H}_T + \bar{U}\hat{H}_X + \bar{U}_X \hat{H} + \bar{H}\hat{U}_X = 0, \tag{4.4}$$

and

$$\bar{H}\hat{U}_{XX} + \bar{U}_X \hat{H}_X + \tfrac{1}{4}\bar{C}^{-1}\bar{H}\hat{H}_{XXX} - \tfrac{1}{4}\bar{A}\bar{H}\Phi'(\bar{H})\hat{H}_X = 0. \tag{4.5}$$

Realizing that $\bar{H}_X = \bar{U}_{XX} = 0$, the above equations are combined into a single equation by differentiating (4.4) with x and substituting for $\bar{H}\hat{U}_{XX}$ from (4.5). The result is a linear advection–diffusion equation for $Y \equiv \hat{H}_X$:

$$Y_T + \bar{U}Y_X = DY_{XX} + \left(V - \bar{U}_X\right) Y, \tag{4.6}$$

with coefficients

$$D = \frac{\bar{H}}{4\bar{C}} \quad \text{and} \quad V = \frac{3\bar{A}}{32\bar{H}^3} \tag{4.7}$$

accounting for the stabilizing effect of surface tension and the destabilizing effect of van der Waals attractions, respectively. It is also apparent from the term $\bar{U}_X Y$ on

the right-hand side that the drainage flow is stabilizing. The latter effect is illustrated below, where (4.6) is solved for the two cases: $Q=0$ and $Q>0$.

4.1. *Uniform film with constant thickness ($Q=0$)*

Here we examine the stability of the basic state $\bar{U}=0$ and $\bar{H}=1$. In this case, all of the coefficients in (4.6) are constant, permitting solutions of the form $Y=\eta(x)\mathrm{e}^{\sigma t}$, where the growth rate σ and function $\eta(x)$ are determined by solving the eigenvalue problem

$$D\eta'' + V\eta = \sigma\eta.$$

We allow the perturbations to the film thickness to be free at the edges of the film: $\eta(\pm 1)=0$, recalling that $Y=\hat{H}_X$. The eigenvalue problem yields two linearly independent solutions:

$$\eta_n^{(1)} = \cos(\alpha_n x), \quad \sigma_n^{(1)} = -\alpha_n^2 D + V,$$
$$\eta_n^{(2)} = \sin(\beta_n x), \quad \sigma_n^{(2)} = -\beta_n^2 D + V,$$

where $\alpha_n=(n-1/2)\pi$ and $\beta_n=n\pi$ for $n\in\mathbb{N}$.

The eigenvalues are real with the maximal eigenvalue given by $\sigma_{max}=\sigma_1^{(1)}$ so that the condition for marginal stability is $\sigma_1^{(1)}=0$. Using the definitions for the coefficients D and V in (4.7), neutral stability is given by

$$\bar{C}\bar{A} = \tfrac{2}{3}\pi^2\bar{H}^4.$$

When expressed in terms of the film aspect ratio $\bar{h}=h_0\bar{H}$ and Sheludko number $S=AC=h_0^4\bar{C}\bar{A}$, the neutral stability condition has form

$$S = \tfrac{2}{3}\pi^2\bar{h}^4. \tag{4.8}$$

Given $\bar{h}$ and S, rupture is predicted to occur if $S>2\pi^2\bar{h}^4/3$.

Vrij (1966) and Ruckenstein & Jain (1974) analysed the stability of a film with infinite horizontal extent, concluding that it is unstable to long waves having wavelengths that exceed a critical value $\lambda_c=4\pi\bar{h}^2\sqrt{2/3S}$, which expresses (1.1) in the present notation. A critical thickness can be estimated from this condition by equating the critical wavelength to the film length, viz. $\lambda_c=2$. Note that this estimate leads to a condition similar to (4.8), where $S\sim\bar{h}^4$ still holds; however, the coefficient $2/3$ is replaced with $8/3$. The coefficients differ because the boundary conditions imposed at the edges of the film are not the same in these two cases and were chosen arbitrarily.

4.2. *Uniformly thinning film ($Q>0$)*

Since the film is thinning for $Q>0$, this leads to a basic state which is time-dependent. For drainage induced by Plateau border suction, the flow rate Q is given by (2.7), which is written in the rescaled variables as

$$\bar{Q} = \frac{3}{8}\sqrt{\frac{2\bar{H}^3}{\alpha}}, \tag{4.9}$$

where $\alpha=a/a_0$ is taken as a parameter which adjusts the strength of flow. We assume that thinning occurs slowly when compared to the growth of the disturbances leading to rupture. As described in § 3, this assumption facilitates a frozen-time approximation,

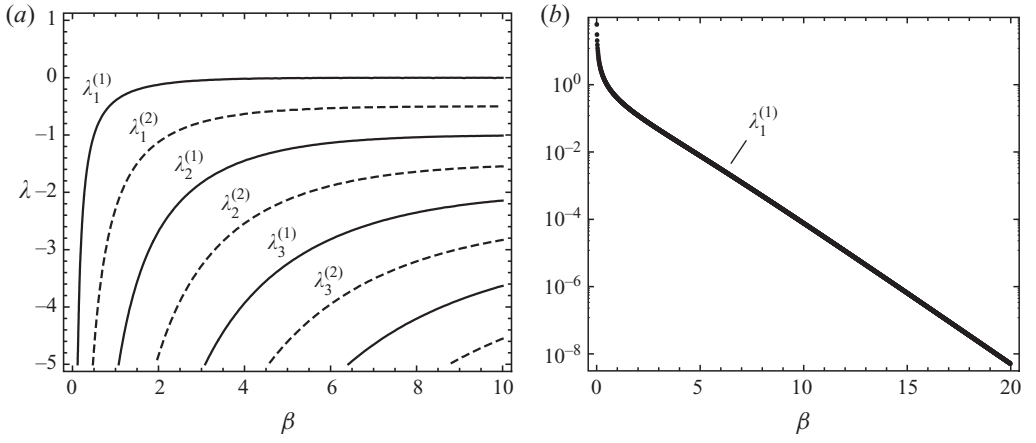

FIGURE 6. (*a*) Two sets of eigenvalues, $\lambda_i^{(1)}$ and $\lambda_i^{(2)}$. (*b*) The maximal eigenvalue $\lambda_1^{(1)}$ decays exponentially to zero as $\beta \to \infty$.

so that $\bar{H} = \bar{H}(t^*)$ and $\bar{U} = \bar{U}(X, t^*)$ at the frozen time t^*. The solutions to (4.6) then take the form

$$Y = \eta(X, t^*)\mathrm{e}^{\sigma(t^*)T},$$

reducing the equation to an eigenvalue problem for the growth rate $\sigma(t^*)$ and spatial mode $\eta(X, t^*)$:

$$D\eta'' - U^* X\eta' + (V - U^*)\eta = \sigma\eta, \tag{4.10}$$

where $U^* = (3/8)\sqrt{2\bar{H}/\alpha}$ is the flow strength. Again, we assume that the ends of the film are free so that $\eta(\pm 1, t^*) = 0$. (Below, the dependence on t^* is dropped to simplify notation.)

Under the change of variables $\eta(X) = W(\xi)$, with $\xi = U^* X^2/2D$, (4.10) is transformed to Kummer's equation (for example, see Lebedev 1972)

$$\xi W'' + \left(\tfrac{1}{2} - \xi\right) W' - \lambda W = 0,$$

where $\lambda = (\sigma - V + U^*)/2U^*$. There exist two linearly independent solutions

$$\eta^{(1)}(X;\lambda) = \mathscr{M}\left(\lambda, \tfrac{1}{2}; \beta X^2\right) \quad \text{and} \quad \eta^{(2)}(X;\lambda) = X\mathscr{M}\left(\tfrac{1}{2} + \lambda, \tfrac{3}{2}; \beta X^2\right), \tag{4.11}$$

where $\mathscr{M}(a, b; \xi)$ denotes a confluent hypergeometric function and $\beta = U^*/2D$. Since (4.10) along with the boundary conditions can be expressed in the form of a self-adjoint eigenvalue problem, if follows that λ, and hence σ, are real numbers. The eigenvalues λ are obtained by ensuring that solutions are compatible with the boundary conditions. For non-trivial solutions, the compatibility conditions

$$\mathscr{M}\left(\lambda^{(1)}, \tfrac{1}{2}; \beta\right) = 0 \quad \text{and} \quad \mathscr{M}\left(\tfrac{1}{2} + \lambda^{(2)}, \tfrac{3}{2}; \beta\right) = 0$$

produce two sets of eigenvalues $\lambda^{(1)}$ and $\lambda^{(2)}$. These are plotted in figure 6(*a*) for a range of β.

It follows from figure 6 that the maximal growth rate corresponds to the eigenvalue $\lambda_1^{(1)}$ through

$$\sigma_{max} = \left(2\lambda_1^{(1)} - 1\right)U^* + V. \tag{4.12}$$

According to the definition $\beta = (3\bar{C}/4)\sqrt{2/\alpha\bar{H}}$, the values $\beta \gg 1$ are most relevant here, because rupture occurs as $\bar{H} \to 0$. We show in figure 6(*b*) that $\lambda_1^{(1)} \sim \mathrm{e}^{-\beta}$ in

this limit, and for our purposes we take $\lambda_1^{(1)} = 0$. Using this result with (4.12), neutral stability is defined by $\sigma_{max} = 0$, yielding

$$\bar{A} = 4\sqrt{2/\alpha}\,\bar{H}^{7/2}.$$

It is convenient to rewrite this in terms of the Sheludko number $S = AC$ and film aspect ratio $\bar{h} = h_0\bar{H}$ for comparison with later results. Using the velocity scale for capillary drainage $U_0 = (\sigma/\mu)\sqrt{h_0/a_0}$ introduced in § 2.2, the neutral stability condition is rewritten as

$$S = 4\sqrt{2/a}\,\bar{h}^{7/2}. \tag{4.13}$$

Alternatively, if we define neutral stability using the effective growth rate given by (3.5), taking $\sigma_{max} = \bar{Q}/\bar{H}$, then we obtain

$$S = 8\sqrt{2/a}\,\bar{h}^{7/2}. \tag{4.14}$$

When the thinning rate is taken into account, the onset of rupture is slightly delayed.

Note that drainage is assumed to occur from Plateau border suction, which produces a higher flow rate as the Plateau border radius a is decreased. The dependence on a in (4.13) and (4.14) indicates that the film is stabilized by an increased flow rate. Moreover, by comparing the neutral stability conditions for the two cases $Q = 0$ and $Q > 0$, the dependence on the film aspect ratio $\bar{h}$ is different. We find that $S \sim \bar{h}^4$ when $Q = 0$ and $S \sim \bar{h}^{7/2}$ when $Q > 0$. This confirms that flow has a stabilizing effect in film rupture. Similar conclusions are drawn by Gumerman & Homsy (1975) and Sharma & Ruckenstein (1987), who also treated drainage flows in their stability analyses of films with tangentially immobile interfaces. In the next section it is shown that further modification of the marginal stability of thinning liquid films arises when Plateau borders are included explicitly.

5. Instability results

The key results from the numerical solution of (3.3) are now summarized. The primary goal is to quantify the critical conditions for rupture and compare them against the neutral stability results that were obtained in the previous section. First, we begin by describing several qualitative features of the solutions to the eigenvalue problem. It was pointed out in § 3 that if an initially stable basic state is set in motion by incrementally decreasing the lamellar thickness h_L, then film rupture can be examined by computing the growth rates and eigenfunctions (modes) from (3.3) at each instant. Stability is monitored through the growth rate with maximal real part, labelled σ_{max}, and corresponding eigenfunctions. A typical set of results from this calculation is illustrated in figure 7, where $\mathrm{Re}(\sigma_{max})$ (a) and $\mathrm{Im}(\sigma_{max})$ (b) are plotted versus the lamellar thickness for a range of Sheludko numbers S and prescribed Plateau border radius $a = 1$. This figure is discussed further below.

5.1. *Qualitative features*

In general, one of the potential difficulties of analysing the linear stability of an approximate basic state originates from the truncation errors $\bar{\psi} - \psi^c$ which are represented in the linear stability equations. Due to this fact, it is important to distinguish between the principle modes of instability and spurious modes that arise from these truncation errors in order to interpret the results. This is possible here since the magnitude of the errors in the basic state vanishes as $h_L \to 0$, whereas the van der Waals attractions which generate the instability are enhanced in this

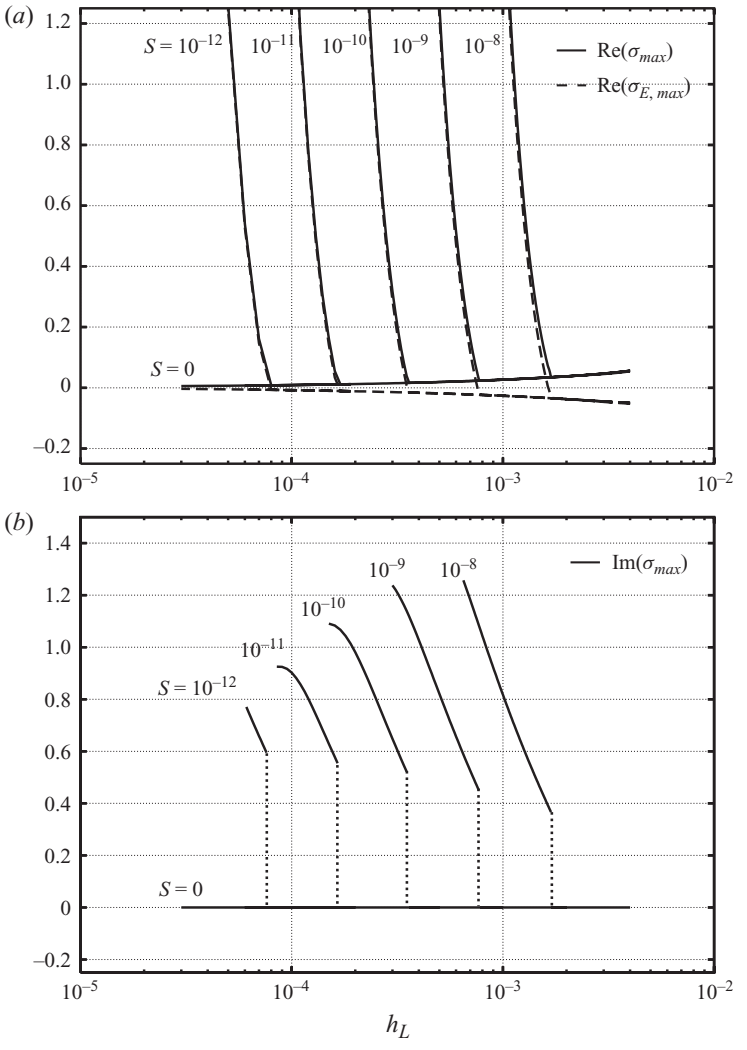

FIGURE 7. (*a*) Real and (*b*) imaginary parts of the maximal growth rate, plotted versus lamellar thickness for physically relevant values of S. As the lamella thins (h_L decreases), growth rates are initially real, with small magnitude; this is spurious growth due to thinning and truncation errors in the basic state. Below a critical h_L, the growth rate has a rapidly increasing real part and a non-zero imaginary part, appearing as a jump; this growth is the result of van der Waals instability. The maximal effective growth rate $\sigma_{E,max}$ (dashed) defined by (3.5) shows a slight delay in the onset of instability.

limit; the two effects become decoupled. To illustrate, compare the case $S = 0$, where van der Waals attractions are excluded, to the cases with $S > 0$ in figure 7(*a*). When $S = 0$, truncation errors lead to disturbances with a small, but positive growth rate which diminishes as $h_L \to 0$. These growth modes are called spurious and they do not lead to rupture. The very same trend is observed for $S > 0$ as the film thickness is initially decreased; however, when h_L decreases below a critical value, Re(σ_{max}) increases rapidly, signalling the van der Waals instability. Rupture modes may be excited before these critical points; however, when accounting for thinning using

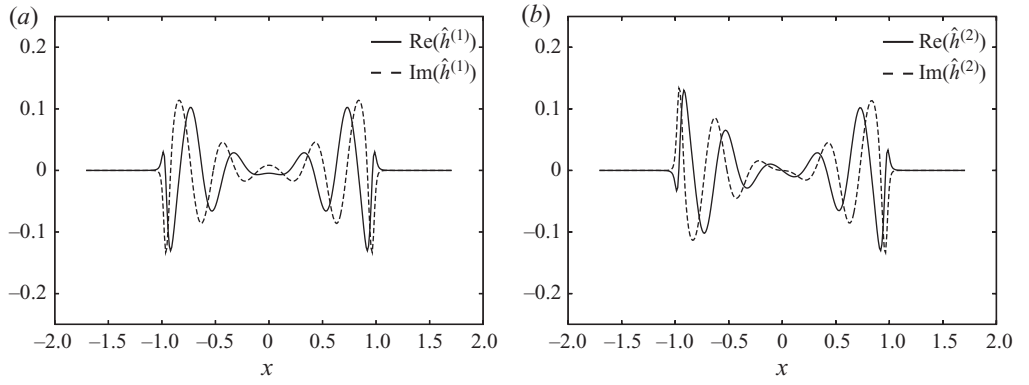

FIGURE 8. A degenerate pair of unstable modes is produced at the onset of rupture (plus complex conjugates). These modes are (*a*) symmetric and (*b*) antisymmetric with respect to $x = 0$. Here, $S = 10^{-9}$ and $a = 1$.

(3.5), their effective growth rate is shown to have negative real part (see dashed lines in figure 7*a*).

Another indicator of the onset of van der Waals instability is that the maximal growth rate passes into the right-half of the complex plane with a non-zero imaginary part. Note that $\mathrm{Im}(\sigma_{max})$ in figure 7(*b*) undergoes a jump as h_L is decreased below the critical value, because the initially dominant spurious modes have $\mathrm{Im}(\sigma_{max}) = 0$. For all of the parameters that we have examined, σ_{max} is a degenerate eigenvalue near rupture onset, paired with two modes $\hat{\psi}^{(1)}$ and $\hat{\psi}^{(2)}$ plus complex conjugates. For example, the real and imaginary parts belonging to $\hat{h}^{(1)}$ and $\hat{h}^{(2)}$, which are the corresponding perturbations to the gas–liquid interface, are plotted in figure 8 for $S = 10^{-9}$ and $a = 1$. The mode $\hat{h}^{(1)}$ is symmetric and the mode $\hat{h}^{(2)}$ is antisymmetric with respect to $x = 0$; linear stability analysis does not distinguish between these two modes of rupture. Also note that the amplitudes of these perturbations are largest near $x = \pm 1$, indicating that the edges of the thin film may be most susceptible to rupture even though these regions are not the thinnest. When Plateau borders are not considered, it is difficult to draw conclusions about the specific features of the modes for rupture, since these modes must conform to boundary conditions that are otherwise artificially imposed at the edges of the film. This is true of earlier analyses of film rupture, including the benchmark cases considered in § 4. In effect, the addition of Plateau borders provides a physically correct method for imposing these boundary conditions.

The complex growth rates induced by the van der Waals instability are an indication of travelling waves. Given the growth rate $\sigma = \sigma_r + \mathrm{i}\sigma_i$ and corresponding mode $\Psi = \Psi_r + \mathrm{i}\Psi_i$, a real solution ψ is formed by

$$\psi = \Psi \mathrm{e}^{\sigma t} + \Psi^* \mathrm{e}^{\sigma^* t} = 2\mathrm{e}^{\sigma_r t} \left[\Psi_r \cos(\sigma_i t) - \Psi_i \sin(\sigma_i t)\right], \tag{5.1}$$

with the asterisk indicating a complex conjugate. In general, the terms in square brackets produce either standing or travelling waves. Taking $\sigma = \sigma_{max}$ and using each of $\hat{h}^{(1)}$ and $\hat{h}^{(2)}$ in place of Ψ, symmetric and antisymmetric waves are plotted for a sequence of times in figure 9, illustrating that it is possible to construct travelling waves. Disturbances to the gas–liquid interface propagate from the centre of the lamella outwards towards its edges, which suggests that they are advected by the flow. To the best of our knowledge, there are no previous stability analyses which predict

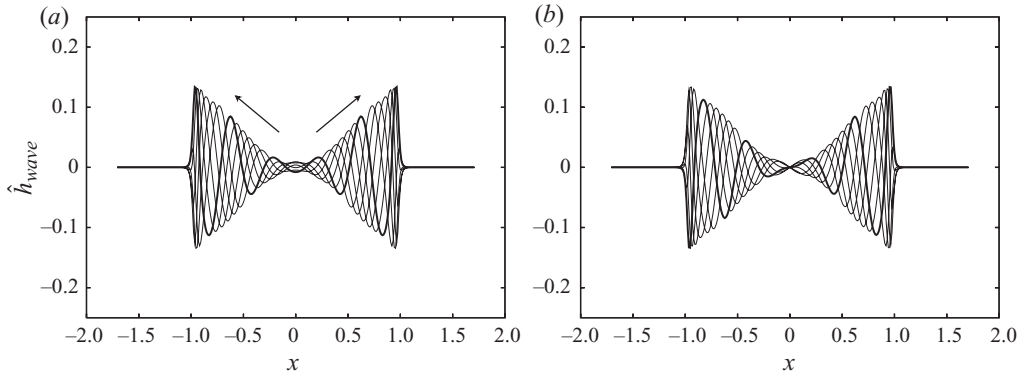

FIGURE 9. The waves given in (5.1) are plotted for the perturbations to the gas–liquid interface for a sequence of times: $\hat{h}_{wave} = \hat{h}_r \cos(\sigma_i t) + \hat{h}_i \sin(\sigma_i t)$. Symmetric waves are shown in (*a*) and antisymmetric waves in (*b*). Unstable disturbances are advected outwards by the drainage flow to the edges of the thin film ($x = \pm 1$). Disturbances are negligible in the Plateau border regions.

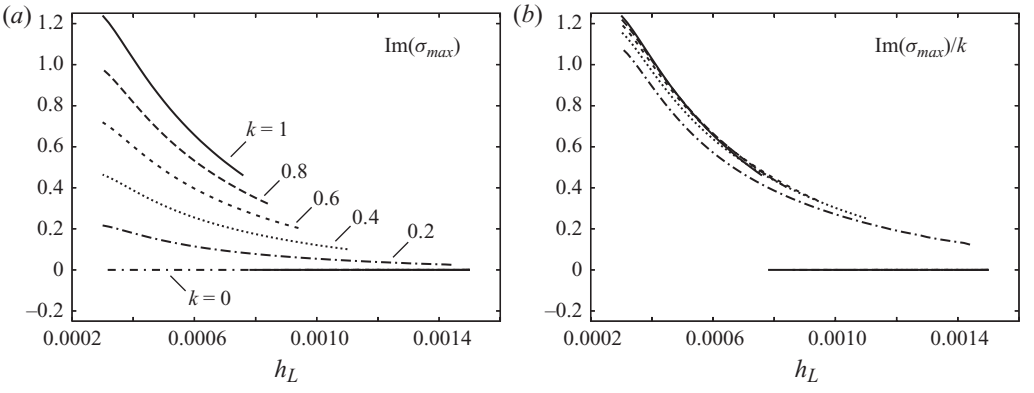

FIGURE 10. (*a*) The imaginary part of σ_{max} is plotted versus lamella thickness for several values of flow strength k defined in (5.2). (*b*) The proportionality between $\mathrm{Im}(\sigma_{max})$ and k. Here, $S = 10^{-9}$ and $a = 1$.

travelling waves. Indeed, without Plateau borders, the stability analysis of a thinning film in § 4.2 does not predict travelling waves.

We can test whether the drainage flow is responsible for producing the travelling waves. For this to be the case, the imaginary part of the growth rate must be proportional to the strength of the flow in the basic state. We have checked for this dependence by introducing an artificial parameter k that modifies the flow in the basic state, viz.

$$\bar{u} = k u^c \quad \text{and} \quad \bar{w} = k w^c, \tag{5.2}$$

where u^c and w^c are the composite solutions given by (2.11) and (2.12); $k = 1$ corresponds to the physical flow. The same calculations were performed with (3.3), choosing $k \in [0, 1]$, and the resulting plots of $\mathrm{Im}(\sigma_{max})$ in figure 10 confirm the proportionality with k. In particular, $\mathrm{Im}(\sigma_{max}) \equiv 0$ when $k = 0$ for all h_L examined. Of course, the cases with $k \neq 1$ are not physical, but they do confirm that travelling waves can be directly attributed to the underlying drainage flow and indeed are completely suppressed in the absence of flow ($k = 0$).

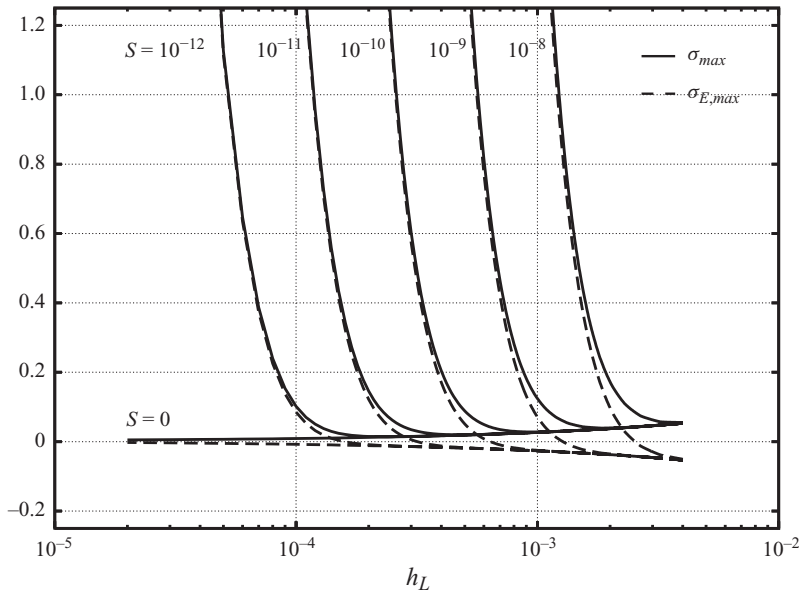

FIGURE 11. The maximal growth rate for the case $k = 0$, where the Plateau borders are present ($a = 1$), but there is no drainage flow. The effective growth rates are plotted as dashed curves, assuming that thinning still occurs.

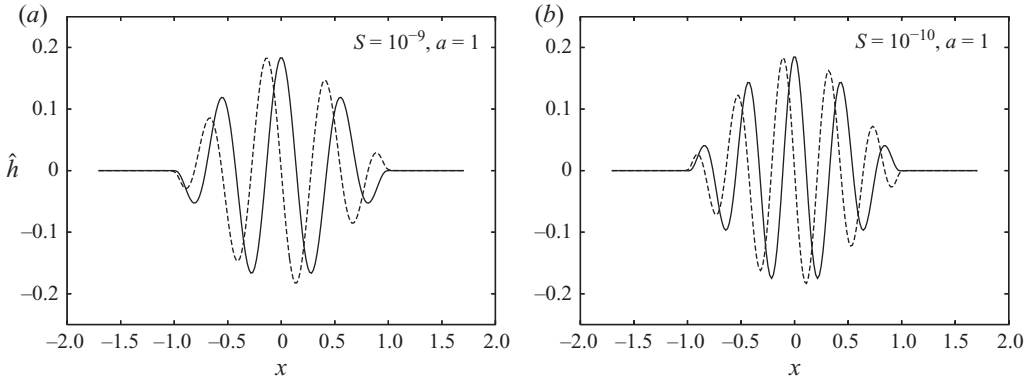

FIGURE 12. Neutrally stable ($\sigma_{E,max} \approx 0$) perturbations to the gas–liquid interface for the case without drainage flow ($k = 0$). The symmetric (—) and antisymmetric (- -) modes are degenerate and the centre of the film appears to be most susceptible to rupture.

The results for the case with $k = 0$ provide an opportunity to study the conditions for rupture without the effects of flow in order to make some comparisons. The maximal growth rate, which is now purely real, is plotted against h_L in figure 11 for a range of S and with $a = 1$, as was done for the full basic state ($k = 1$) in figure 7. By comparing the real part of the effective growth rate in these two figures, locating the points where $\mathrm{Re}(\sigma_{E,max}) = 0$, it can be seen that rupture is delayed when there is a drainage flow present. Flow was also shown to enhance film stability in § 4.2 and this has been further established in the literature for related problems (Gumerman & Homsy 1975; Sharma & Ruckenstein 1987; Coons *et al.* 2003). The modes of rupture for the case with $k = 0$ are shown in figure 12. It is interesting to compare

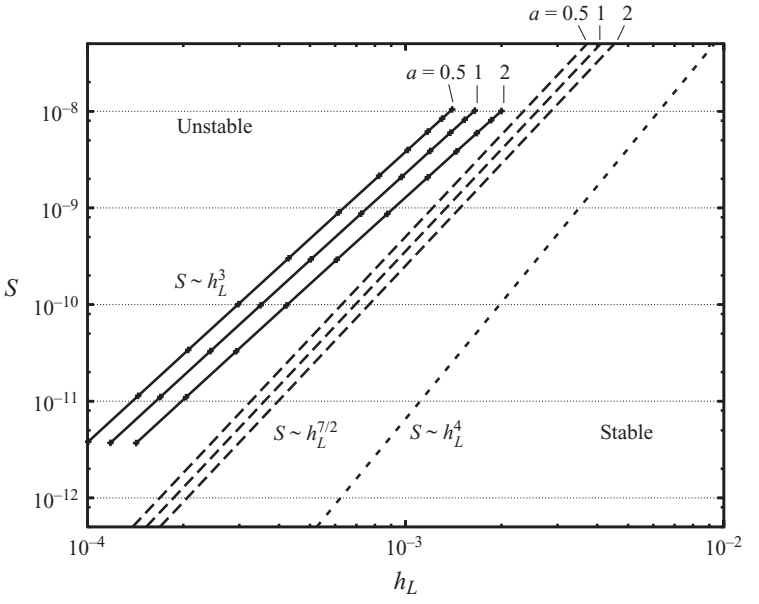

FIGURE 13. Neutral stability curves showing the power-law dependence of the critical thickness on S (log–log axes) for the finite length film with constant thickness given by (4.8) (short dashes), the uniformly thinning film of finite length given by (4.14) (long dashes) and the full basic state given by (5.4) (the points were obtained numerically and follow $S \sim h_L^3$, plotted as a solid line). The film is predicted to be unstable when h_L lies to the left of a given neutral stability curve.

these modes with those shown in figure 8 for $k = 1$. Once again, the van der Waals instability produces a pair of modes which are symmetric and antisymmetric with respect to $x = 0$. In the case where $k = 0$, however, the most susceptible region for rupture appears to be at the centre of the lamella rather than at the edges. It is clear by now that flow leads to several distinct qualitative features in the rupture process.

5.2. *Neutral stability: critical conditions for rupture*

We identify the conditions for neutral stability using the real part of the effective growth rate defined by (3.5), viz.

$$\mathrm{Re}(\sigma_{E,max}) = 0 \quad \Longrightarrow \quad \mathrm{Re}(\sigma_{max}) = Q/h_L. \tag{5.3}$$

By fixing the Plateau border radius a, the marginally stable film thickness was calculated for several values of S and these points are plotted in figure 13. Alongside these results, we plot the neutral stability curves for both the benchmark problems given by (4.8) and (4.14). Note that a film is predicted to rupture spontaneously when the (instantaneous) thickness lies to the left of a given curve. From the numerical calculations using the full basic state, we find that there is a power-law dependence between S and h_L at neutral stability:

$$S = f(a)h_L^3, \tag{5.4}$$

where the dependence on a is discussed separately below. The benchmarks lead to different power-law dependences between S and h_L, where $S \sim h_L^{7/2}$ in (4.13) for the case with thinning and $S \sim h_L^4$ in (4.8) for the case without thinning. The full basic

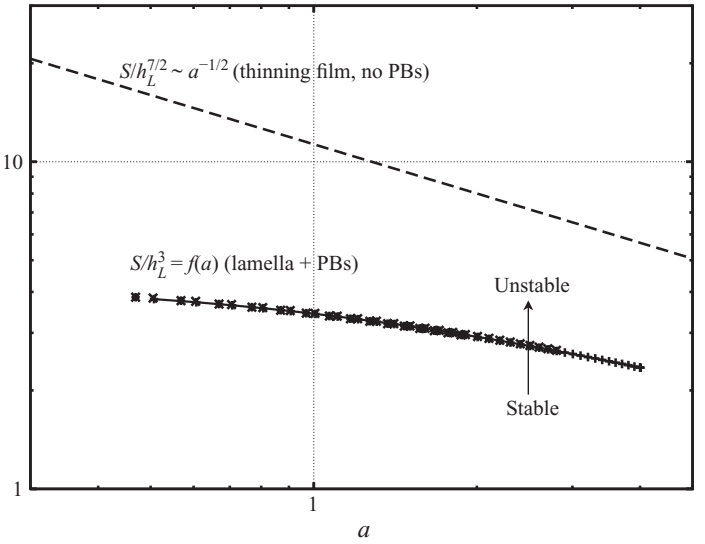

FIGURE 14. The neutral stability curves show the dependence on a given by (5.4) for the full basic state (solid line) and by (4.14) for the thinning film without Plateau (dashed line). For the full basic state, $S = 10^{-8}$, 10^{-9} and 10^{-10} are all plotted and collapse onto the same curve.

state is found to be more stable than either of the benchmark cases and the degree of stabilization increases as the Sheludko number decreases.

The dependence on a in (4.14) and (5.4) is shown in figure 14. In the case of (5.4), neutral stability was calculated for several values of S and all the results collapse onto the single curve $f(a) = S/h_L^3$. Recall from (2.7) that the flow rate produced by Plateau border suction is directly proportional to $a^{-1/2}$ and the same dependence occurs in the neutral stability condition given by (4.14) for the thinning film with uniform thickness (no Plateau borders), thus demonstrating the direct stabilizing effect of flow for this idealized basic state. In the case of the full basic state, the parameter a not only controls the rates of thinning and drainage, but also specifies the curvature of the Plateau borders, and hence the shape of the lamella at its edges. The dependence on a in (5.4) is more complicated and, in particular, it is possible that the critical lamellar thickness approaches a minimum value for smaller values of a, though this has not been investigated. In the next section, we discuss some possible mechanisms to explain the stabilization shown in figures 13 and 14.

6. Discussion

Using approximate parameter values for water, aniline and molten aluminium, the predictions for the critical thickness are compared in table 1 for the full basic state (labelled h_L^{crit}) and both benchmark cases (h_1 and h_2). The values are reported for films of lengths (a) 0.1 cm and (b) 0.01 cm, for values of S which range over approximately three orders of magnitude, and for $a = 1$. Note that in all cases, the shorter film is more stable as expected. The predictions for h_L^{crit} show quantitatively the degree of stabilization over the benchmark predictions. For example, consider an aluminium foam with a lamella of length 0.1 cm. We have that $h_L^{crit} = 26$ nm and that $h_1 = 280$ nm for a film with the same length but of constant thickness – a difference of one order of magnitude. Even when flow and thinning are added to the basic state, the prediction $h_2 = 90$ nm is larger than h_L^{crit} by over a factor of 3.

Substance	S ($\times 10^{12}$)	h_1 (nm)	h_2 (nm)	h_L^{crit} (nm)
Water				
(*a*)	0.07	330	110	32
(*b*)	7.4	100	40	15
Aluminium				
(*a*)	0.04	280	90	26
(*b*)	4.0	88	34	12
Aniline				
(*a*)	0.86	600	220	72
(*b*)	86	190	81	34

TABLE 1. A comparison of the critical thicknesses (in nanometres) for films with lengths (*a*) $L_0 = 0.1$ cm and (*b*) $L_0 = 0.01$ cm, choosing $a = 1$ for the (dimensionless) Plateau border radius. Here, h_1 is calculated from (4.8), h_2 from (4.14) and h_L^{crit} are values calculated from (5.4) for the full basic state.

To our knowledge, there are currently no experimental measurements of critical thicknesses for pure liquid films reported in the literature. Banhart *et al.* (2001) used X-ray techniques to observe single-rupture events in foams made of molten aluminium; however, in order to limit drainage, solid particles were suspended in the liquid phase. Perhaps coincidentally, they report critical film thicknesses which are comparable to the particle size (ca. 50 μm). There are several experimental studies of the critical thickness for foam films containing surfactants and emulsion films (for a recent review, see Manev & Nguyen 2005). Even though the surfaces of these films are not completely mobile and other effects like surface elasticity may be involved, these experiments provide us with a point of reference. For instance, Vrij (1966) compiled measurements taken by Sheludko and coworkers for surfactant-stabilized aniline and aqueous films ($L_0 = 0.01$ cm) reporting critical thicknesses of 42 and 27 nm, respectively. These values are close to the corresponding values of h_L^{crit} listed in table 1, though the value of a in these experiments is uncertain. There are, however, some important differences when tangential stresses are present at the interfaces of the film. We discuss these and possible generalizations to our stability analysis in more detail below.

In light of the predictions in table 1, we return to an assumption made earlier to derive the basic state in § 2.2, where it was assumed that capillary suction is the only effect driving thinning; however, based on the small values for h_L^{crit}, especially for shorter films ($L_0 \ll 0.1$ cm), this is not likely to be the case. As a lamella approaches its critical thickness, the rate of thinning will be enhanced to some degree by the van der Waals attractions. We do not provide an estimate for this additional effect, but simply comment that, given an increased flow rate for drainage as well as the definition for the effective growth rate in (3.5), which is based on the rate of thinning, we would expect the film to be further stabilized if such effects were included. By these arguments, the values for h_L^{crit} reported in table 1 are considered upper bounds.

Comparisons between the van der Waals instability for a lamella with Plateau borders and the simpler benchmark cases indicate that thinning, drainage flow and curved boundaries lead to a more stable film. In the case of thinning, stabilization is inferred from the definition of the effective growth rate (3.5). This definition states that in the immediate vicinity of marginal stability, unstable disturbances require a short but finite time to grow and meanwhile the film continues to thin; it is only when

the growth of the disturbances outpace thinning that the onset of rupture is detected. With respect to the drainage flow, stabilization could be manifested in a couple of ways. Firstly, as disturbances are advected by the flow to the edges of the thin film near the Plateau borders, they are moved to a thicker and presumably more stable region of the film. Interestingly, the lamellar edges appear to be the most susceptible to rupture. Secondly, as disturbance waves are pushed towards the Plateau borders they become compressed and consequently stabilized by surface tension (see figures 8 and 9). This 'wave shortening' mechanism is one possible interpretation of an earlier finding by Sharma & Ruckenstein (1987), who reported that long waves are more strongly stabilized when a drainage flow is present.

Due to our interest in metallic foams, for which no surfactants are available, we have analysed the rupture of free films composed of pure liquids. We have therefore presented a stability analysis for the limiting case in which the gas–liquid interfaces are stress-free. As we mentioned above, surface tractions are often present in dispersed systems, including foams which contain surfactant and emulsions. Curved boundaries, drainage flows and thinning are, however, ubiquitous features of the thin films formed in these systems. Based on the findings of this paper, the importance of these features on film rupture motivates the systematic incorporation of Plateau borders into other theoretical treatments of film stability in dispersed systems. We conclude this paper with a brief discussion of how an approach similar to the one used here could be generalized to study these systems.

It has been established that when a fluid drains from a tangentially immobile film into the adjoining Plateau borders, the film profile is non-monotonic due to localized constrictions in the film near the Plateau borders (Frankel & Mysels 1962; Jones & Wilson 1978; Joye, Miller & Hirasaki 1992; Aradian, Raphael & de Gennes 2001; Howell & Stone 2005). This feature has been referred to as 'marginal pinching' by some authors (e.g. Aradian *et al.* 2001) and 'hydrodynamic non-homogeneity' by others (e.g. Coons *et al.* 2003), and it marks an important difference from the case with stress-free interfaces, where only monotonic film profiles are possible (see figure 3 as well as Howell & Stone 2005). (These 'hydrodynamic' constrictions are of a different origin than those predicted here, where constrictions at the film edges arise from van der Waals instability which is 'non-hydrodynamic' in origin.) An approximate basic state which includes marginal pinching can be derived using a matched asymptotic analysis similar to that described in § 2.2 and in Brush & Davis (2005). Aradian *et al.* (2001) provide the framework for such an analysis through a decomposition of the domain into a flat film region, a pinched region and a capillary-static Plateau border region; however, they have obtained solutions only for a semi-infinite film region. Interestingly, Breward & Howell (2002) performed the same analysis for a film of finite length containing soluble surfactant and found that both monotonic and non-monotonic profiles are possible, but were not able to identify a clear transition between the two types of solutions. The construction of a basic state for the limiting case with tangentially immobile interfaces appears to be more straightforward than for their model. Given this basic state, a full linear stability analysis could be performed via the algorithm described in § 3.

The authors would like to thank Dr M. Gratton for many useful discussions and Professor A. Bayliss for his crucial advice on the numerical calculations. This material is based upon work supported by the National Science Foundation under Grant nos DMS-0636574 (A.M.A.), CMMI-0827101 (L.N.B.) and CMMI-0826703 (S.H.D.).

Appendix. Linear stability equations in boundary-fitted curvilinear coordinates

Consider a general curvilinear coordinate system $\xi = \xi(x, z, t)$ and $\zeta = \zeta(x, z, t)$ which maps the linearized physical domain into the fixed rectangular domain $1 \leqslant \xi \leqslant M$, $1 \leqslant \zeta \leqslant N$. For an infinitesimal perturbation $\hat{h} = h - \bar{h}$ to the gas–liquid interface,

$$z = \bar{h}(x, t) + \hat{h}(x, t) \quad \mapsto \quad \zeta = N + \hat{f}(\xi, t),$$

where $|\hat{f}| \ll N$. The resulting perturbations to the field variables are written as

$$p = \bar{p} + \hat{p} \quad \text{and} \quad \boldsymbol{v} = \bar{\boldsymbol{v}} + \hat{\boldsymbol{v}},$$

where $\bar{\boldsymbol{v}} = \bar{u}\boldsymbol{a}_1 + \bar{w}\boldsymbol{a}_2$ and $\hat{\boldsymbol{v}} = \hat{u}\boldsymbol{a}_1 + \hat{w}\boldsymbol{a}_2$ are the contravariant components of the basic state and perturbed velocity fields with the base vectors $\boldsymbol{a}_1 = (x_\xi, z_\xi)$ and $\boldsymbol{a}_2 = (x_\zeta, z_\zeta)$ tangential to the coordinate lines. From these base vectors we obtain the metric tensor and Jacobian for this coordinate transformation:

$$g_{ij} = \boldsymbol{a}_i \cdot \boldsymbol{a}_j \quad \text{and} \quad J = \sqrt{\det(g_{ij})},$$

respectively. Here, the base vectors are positively oriented so that $\det(g_{ij}) > 0$ at all points of interest.

With these definitions, linearize the field equations and boundary conditions (2.1)–(2.6) expressed in the coordinate system defined above. First, the perturbations to the flow field satisfy the following continuity equation:

$$\frac{\partial}{\partial \xi}(J\hat{u}) + \frac{\partial}{\partial \zeta}(J\hat{w}) = 0. \tag{A 1}$$

For the momentum balance given by (2.1), it is convenient to introduce the reduced pressure $\Pi = p + \phi(h)$. As shown below, the contributions from van der Waals attractions ϕ are expressed in the jump in normal stress at the gas–liquid interface. We consider the contravariant components of perturbations to momentum, which yields the ξ-component of momentum

$$\begin{aligned} g_{22}\frac{\partial \hat{\Pi}}{\partial \xi} - g_{12}\frac{\partial \hat{\Pi}}{\partial \zeta} = {} & J\frac{\partial}{\partial \xi}\left[J^{-1}\left(g_{22}\hat{v}^1_{;1} - g_{12}\hat{v}^1_{;2}\right)\right] - J\frac{\partial}{\partial \zeta}\left[J^{-1}\left(g_{12}\hat{v}^1_{;1} - g_{11}\hat{v}^1_{;2}\right)\right] \\ & + \left(g_{22}\Gamma^1_{11} - g_{12}\Gamma^1_{12}\right)\hat{v}^1_{;1} + \left(g_{11}\Gamma^1_{12} - g_{12}\Gamma^1_{11}\right)\hat{v}^1_{;2} \\ & + \left(g_{22}\Gamma^1_{12} - g_{12}\Gamma^1_{22}\right)\hat{v}^2_{;1} + \left(g_{11}\Gamma^1_{22} - g_{12}\Gamma^1_{12}\right)\hat{v}^2_{;2}, \end{aligned} \tag{A 2}$$

and the ζ-component of momentum

$$\begin{aligned} g_{11}\frac{\partial \hat{\Pi}}{\partial \zeta} - g_{12}\frac{\partial \hat{\Pi}}{\partial \xi} = {} & J\frac{\partial}{\partial \xi}\left[J^{-1}\left(g_{22}\hat{v}^2_{;1} - g_{12}\hat{v}^2_{;2}\right)\right] - J\frac{\partial}{\partial \zeta}\left[J^{-1}\left(g_{12}\hat{v}^2_{;1} - g_{11}\hat{v}^2_{;2}\right)\right] \\ & + \left(g_{22}\Gamma^2_{11} - g_{12}\Gamma^2_{12}\right)\hat{v}^1_{;1} + \left(g_{11}\Gamma^2_{12} - g_{12}\Gamma^2_{11}\right)\hat{v}^1_{;2} \\ & + \left(g_{22}\Gamma^2_{12} - g_{12}\Gamma^2_{22}\right)\hat{v}^2_{;1} + \left(g_{11}\Gamma^2_{22} - g_{12}\Gamma^2_{12}\right)\hat{v}^2_{;2}, \end{aligned} \tag{A 3}$$

where

$$\hat{\Pi} = \hat{p} + \frac{\phi'(\bar{h})\bar{h}}{N-1}\hat{f} \tag{A 4}$$

are the perturbations to the reduced pressure. Here, the terms $\hat{v}^i_{;j}$ are the components of the gradient (covariant derivative) $\nabla\hat{\boldsymbol{v}}$ of the velocity perturbations. In general, for a two-dimensional contravariant vector field $\boldsymbol{v} = v^1\boldsymbol{a}_1 + v^2\boldsymbol{a}_2$, covariant differentiation

leads to a rank-two tensor with components

$$v^1_{;1} = \frac{\partial v^1}{\partial \xi} + \Gamma^1_{11} v^1 + \Gamma^1_{12} v^2, \qquad v^1_{;2} = \frac{\partial v^1}{\partial \zeta} + \Gamma^1_{12} v^1 + \Gamma^1_{22} v^2,$$
$$v^2_{;1} = \frac{\partial v^2}{\partial \xi} + \Gamma^2_{11} v^1 + \Gamma^2_{12} v^2, \qquad v^2_{;2} = \frac{\partial v^2}{\partial \zeta} + \Gamma^2_{12} v^1 + \Gamma^2_{22} v^2,$$

where Γ^k_{ij} denote Christoffel symbols of the second kind (for example, see Aris 1989).

The interfacial boundary conditions are enforced at $\zeta = N + \hat{f}(\xi, t)$ in the mapped domain and linearization is performed through a Taylor expansion about $\zeta = N$. In this way, the following linearized normal and tangential stress conditions at $\zeta = N$ are obtained:

$$\hat{\Pi} - \frac{\phi'(\bar{h})\bar{h}}{N-1}\hat{f} - \hat{\tau}_{nn} - C^{-1}\hat{\mathscr{K}} + \frac{\partial}{\partial \zeta}(\bar{p} - \bar{\tau}_{nn} - C^{-1}\bar{\mathscr{K}})\hat{f} = 0, \tag{A 5}$$

$$\hat{\tau}_{nt} + \frac{\partial}{\partial \zeta}(\bar{\tau}_{nt})\hat{f} = 0, \tag{A 6}$$

where the definition for the reduced pressure given by (A 4) is used in the normal stress balance. Here, $\bar{\mathscr{K}}$ and $\hat{\mathscr{K}}$ are terms for interfacial curvature, given by

$$\bar{\mathscr{K}} = J^{-1}\left\{\frac{\partial}{\partial \zeta}(g_{11})^{1/2} - \frac{\partial}{\partial \xi}\left[g_{12}(g_{11})^{-1/2}\right]\right\}, \quad \hat{\mathscr{K}} = J^{-1}\frac{\partial}{\partial \xi}\left[J^2(g_{11})^{-3/2}\hat{f}_\xi\right],$$

and $\bar{\tau}_{nn}$, $\hat{\tau}_{nn}$, $\bar{\tau}_{nt}$ and $\hat{\tau}_{nt}$ are terms for viscous normal stresses (nn) and viscous shear stresses (nt), given by

$$\begin{aligned}
\bar{\tau}_{nn} &= -2g_{12}(g_{11})^{-1}\bar{v}^2_{;1} + 2\bar{v}^2_{;2},\\
\hat{\tau}_{nn} &= -2g_{12}(g_{11})^{-1}\hat{v}^2_{;1} + 2\hat{v}^2_{;2}\\
&\quad + 2\left[g_{12}(g_{11})^{-1}\left(\bar{v}^1_{;1} - \bar{v}^2_{;2}\right) - \bar{v}^1_{;2} - (g_{11})^{-2}\left(J^2 - (g_{12})^2\right)\bar{v}^2_{;1}\right]\hat{f}_\xi,\\
\bar{\tau}_{nt} &= -g_{12}\left(\bar{v}^1_{;1} - \bar{v}^2_{;2}\right) + g_{11}\bar{v}^1_{;2} + (g_{11})^{-1}\left(J^2 - (g_{12})^2\right)\bar{v}^2_{;1},\\
\hat{\tau}_{nt} &= -g_{12}\left(\hat{v}^1_{;1} - \hat{v}^2_{;2}\right) + g_{11}\hat{v}^1_{;2} + (g_{11})^{-1}\left(J^2 - (g_{12})^2\right)\hat{v}^2_{;1}\\
&\quad - 2J^2(g_{11})^{-1}\left[\bar{v}^1_{;1} - \bar{v}^2_{;2} + 2g_{12}(g_{11})^{-1}\bar{v}^2_{;1}\right]\hat{f}_\xi.
\end{aligned}$$

Finally, the linearized kinematic condition is given by

$$\hat{f}_t = \hat{w} - (\bar{u} - U)\hat{f}_\xi + \frac{\partial}{\partial \zeta}(\bar{w} - W)\hat{f}, \qquad \text{at } \zeta = N, \tag{A 7}$$

where $\boldsymbol{V} = U\boldsymbol{a}_1 + W\boldsymbol{a}_2$ accounts for the motion of the reference frame with components

$$U = (\dot{x}\boldsymbol{i} + \dot{z}\boldsymbol{k}) \cdot \boldsymbol{a}^1 \quad \text{and} \quad W = (\dot{x}\boldsymbol{i} + \dot{z}\boldsymbol{k}) \cdot \boldsymbol{a}^2,$$

where $\dot{x} \equiv \partial x/\partial t$ and $\dot{z} \equiv \partial z/\partial t$ for fixed ξ and ζ and $\boldsymbol{a}^i$ are the contravariant base vectors (i.e. $\boldsymbol{a}^i \cdot \boldsymbol{a}_j = \delta^i_j$). These terms for the motion of the reference frame arise because the evolving physical domain is mapped to a fixed rectangular domain.

Symmetry conditions are imposed at the remaining boundaries (i.e. $\xi = 1, M$ and $\zeta = 1$). These conditions are expressed as

$$\hat{\boldsymbol{v}} \cdot \boldsymbol{n} = 0, \quad \nabla(\hat{\boldsymbol{v}} \cdot \boldsymbol{t}) \cdot \boldsymbol{n} = 0 \quad \text{and} \quad \nabla\hat{p} \cdot \boldsymbol{n} = 0, \tag{A 8}$$

where $\boldsymbol{n}$ and $\boldsymbol{t}$ are the unit normal and unit tangent vectors to the boundary. For example, at the film centreline $\zeta = 1$, this yields

$$\hat{w} = 0,$$
$$g_{12}\frac{\partial}{\partial \xi}(g_{11}\hat{u}) = g_{11}\frac{\partial}{\partial \zeta}(g_{11}\hat{u} + g_{12}\hat{w}),$$
$$g_{22}\frac{\partial \hat{p}}{\partial \xi} = g_{12}\frac{\partial \hat{p}}{\partial \zeta}.$$

Similar conditions are derived from (A 8) at the other boundaries.

REFERENCES

Amestoy, P. R., Duff, I. S., L'Excellent, J.-Y. & Koster, J. 2000 Multifrontal parallel distributed symmetric and unsymmetric solvers. *Comput. Methods Appl. Mech. Engng* **184**, 501–520.

Aradian, A., Raphael, E. & de Gennes, P. G. 2001 'Marginal pinching' in soap films. *Europhys. Lett.* **55**, 834–840.

Aris, R. 1989 *Vectors, Tensors, and the Basic Equations of Fluid Mechanics*. Dover.

Banhart, J. 2001 Manufacture, characterisation, and application of cellular metals and metal foams. *Prog. Mater. Sci.* **46** (6), 559–632.

Banhart, J., Stanzick, H., Helfen, L. & Baumbach, T. 2001 Metal foam evolution studied by synchrotron radioscopy. *Appl. Phys. Lett.* **78** (8), 1152–1154.

Bretherton, F. P. 1961 The motion of long bubbles in tubes. *J. Fluid Mech.* **10**, 166–188.

Breward, C. J. W. & Howell, P. D. 2002 The drainage of a foam lamella. *J. Fluid Mech.* **458**, 379–406.

Brush, L. N. & Davis, S. H. 2005 A new law of thinning in foam dynamics. *J. Fluid Mech.* **534**, 227–236.

Burelbach, J. P., Bankoff, S. G. & Davis, S. H. 1988 Nonlinear stability of evaporating condensing liquid films. *J. Fluid Mech.* **195**, 463–494.

Coons, J. E., Halley, P. J., McGlashan, S. A. & Tran-Cong, T. 2003 A review of drainage and spontaneous rupture in free standing thin films with tangentially immobile interfaces. *Adv. Colloid Interface Sci.* **105**, 3–62.

Davis, S. H. 1976 Stability of time-periodic flows. *Annu. Rev. Fluid Mech.* **8**, 57–74.

Derjaguin, B. 1955 Definition of the concept and determination of the disjoining pressure. *Colloid J. USSR* **17**, 191–197.

Derjaguin, B. & Landau, L. 1941 Theory of the stability of strongly charged lyophobic sols and of the adhesion of strongly charged particles in solutions of electrolytes. *Acta Phys. Chem. USSR* **14**, 633–662.

Diez, J. A. & Kondic, L. 2007 On the breakup of fluid films of finite and infinite extent. *Phys. Fluids* **19**, 072107.

Dzyaloshinskii, I. E., Lifshitz, E. M. & Pitaevskii, L. P. 1960 van der Waals forces in liquid films. *Sov. Phys. JETP* **37**, 161–170.

Dzyaloshinskii, I. E. & Pitaevskii, L. P. 1959 van der Waals forces in an inhomogenous dielectric. *Sov. Phys. JETP* **36**, 1282–1287.

Erneux, T. & Davis, S. H. 1993 Nonlinear rupture of free films. *Phys. Fluids* **5**, 1117–1122.

Frankel, S. P. & Mysels, K. J. 1962 On dimpling during approach of two interfaces. *J. Phys. Chem.* **66**, 190–191.

Gumerman, R. J. & Homsy, G. M. 1975 The stability of radially bounded thin films. *Chem. Engng Commun.* **2**, 27–36.

Howell, P. D. & Stone, H. A. 2005 On the absence of marginal pinching in thin free films. *Eur. J. Appl. Math.* **16**, 569–582.

Ida, M. P. & Miksis, M. J. 1996 Thin film rupture. *Appl. Math. Lett.* **9**, 35–40.

Ivanov, I. B., Radoev, B., Manev, E. & Sheludko, A. 1970 Theory of critical thickness of rupture of thin liquid films. *Trans. Faraday Soc.* **66**, 1262–1273.

Jones, A. F. & Wilson, S. D. R. 1978 Film drainage problem in droplet coalescence. *J. Fluid Mech.* **87**, 263–288.

Joye, J. L., Miller, C. A. & Hirasaki, G. J. 1992 Dimple formation and behavior during axisymmetric foam film drainage. *Langmuir* **8**, 3083–3092.

Lebedev, N. N. 1972 *Special Functions and Their Applications*. Dover.

Lehoucq, R. B., Sorensen, D. C. & Yang, C. 1998 *ARPACK Users' Guide: Solution of Large-Scale Eigenvalue Problems with Implicitly Restarted Arnoldi Methods*. SIAM.

Lifshitz, E. M. 1956 The theory of molecular attractive forces between solids. *Sov. Phys. JETP* **2**, 73–83.

Lucassen, J., van den Tempel, M., Vrij, A. & Hesselink, F. T. 1970 Waves in thin liquid films: 1. Different modes of vibration. *Proc. K. Ned. Akad. Wet.* B **73**, 109.

Manev, E. & Nguyen, A. 2005 Critical thickness of microscopic thin liquid films. *Adv. Colloid Interface Sci.* **114**, 133–146.

Overbeek, J. T. G. 1960 Black soap films. *J. Phys. Chem.* **64**, 1178.

Parsegian, V. A. 2006 *Van der Waals Forces: A Handbook for Biologists, Chemists, Engineers, and Physicists*. Cambridge University Press.

Plateau, J. A. F. 1873 *Statique Expérimentale et Théorique des Liquides Soumis aux Seules Forces Moléculaires*. Gauthier-Villars.

Ruckenstein, E. & Jain, R. K. 1974 Spontaneous rupture of thin liquid films. *J. Chem. Soc. Faraday Trans.* II **70**, 132–147.

Sharma, A. & Ruckenstein, E. 1987 Stability, critical thickness, and the time of rupture of thinning foam and emulsion films. *Langmuir* **3**, 760–768.

Sheludko, A. 1962 Sur certaines particularités des lames mousseuses. *Proc. K. Ned. Akad. Wet.* B **65**, 87.

Sheludko, A. 1967 Thin liquid films. *Adv. Colloid Interface Sci.* **1**, 391–464.

Shen, S. F. 1961 Some considerations on the laminar stability of time-dependent basic flows. *J. Aerosp. Sci.* **28**, 397–404, 417.

Thompson, J. F., Warsi, Z. U. A. & Mastin, C. W. 1985 *Numerical Grid Generation: Foundations and Applications*. Elsevier.

Vaynblat, D., Lister, J. R. & Witelski, T. P. 2001 Rupture of thin viscous films by van der Waals forces: evolution and self-similarity. *Phys. Fluids* **13**, 1130–1140.

Verwey, E. J. W. & Overbeek, J. T. G. 1948 *Theory of the Stability of Lyophobic Colloids*. Elsevier.

Vrij, A. 1966 Possible mechanism for the spontaneous rupture of thin, free liquid films. *Discuss. Faraday Soc.* **42**, 23–33.

Vrij, A., Hesselink, F. T., Lucassen, J. & van den Tempel, M. 1970 Waves in thin liquid films: 2. Symmetrical modes in very thin films and film rupture. *Proc. K. Ned. Akad. Wet.* B **73**, 124.

Vrij, A. & Overbeek, J. T. G. 1968 Rupture of thin liquid films due to spontaneous fluctuations in thickness. *J. Am. Chem. Soc.* **90**, 3074–3078.

Williams, M. B. & Davis, S. H. 1982 Nonlinear theory of film rupture. *J. Colloid Interface Sci.* **90**, 220–228.